Clays and Clay Minerals, Vol. 45, No. 4, 551–563, 1997.

INTERCALATION OF HALLOYSITE: A RAMAN SPECTROSCOPIC STUDY

RAY L. FROST[1] AND JANOS KRISTOF[2]

[1] Centre for Instrumental and Developmental Chemistry, Queensland University of Technology, 2 George Street, GPO Box 2434, Brisbane Queensland 4001, Australia

[2] Department of Analytical Chemistry, University of Veszprem, H8201 Veszprem, PO Box 158, Hungary

Abstract—Intercalates from an ordered halloysite with urea and potassium acetate were studied using Raman microscopy. The urea intercalate showed new Raman bands at 3387, 3410, 3497 and 3598 cm^{-1} which were attributed to the formation of a urea-Si_2O_5 complex. New Raman bands were observed at 3585 and 3602 cm^{-1} for the potassium acetate intercalate with concomitant loss of intensity of the bands at 3635, 3655, 3675 and 3696 cm^{-1}. These new bands were attributed to the hydrogen bonds formed between the acetate and the inner surface hydroxyl groups. Remarkable changes in intensity in the lattice region of the halloysite were observed, the foremost being the reduction of the intensity of the bands at 243, 271 and 336 cm^{-1}. Pronounced changes in the bands at 913 and 143 cm^{-1} attributed to the Al-OH librations were also observed.

It is proposed that 2 distinct types of intercalation were present, as exemplified by: 1) urea intercalate, where the intercalating molecule hydrogen bonds to the Si-O of the halloysite layers and 2) potassium acetate intercalate, where the molecule is hydrogen-bonded to the inner surface hydroxyls of the halloysite layer and interacts with the tetrahedral sheet of the next adjacent halloysite layer. The Raman spectra of the intercalated halloysite strongly resembled that of an intercalated kaolinite.

Key Words—Halloysite, Intercalation, Kaolinite, Raman, Raman Microprobe, X-ray Diffraction.

INTRODUCTION

Intercalation of halloysites has been studied for some time (Ledoux and White 1967; Olejnik et al. 1968) and has been used to distinguish between kaolinites and halloysites (Churchman et al. 1984; Theng et al. 1984). Intercalation has also been used to quantify mixtures of kaolinite and halloysite (Janik and Keeling 1993). Clay minerals can interact with both organic and inorganic chemicals through a number of mechanisms such as adsorption, intercalation and cation exchange. The basic principles of intercalation reactions have been elucidated for kaolinite by Lagaly (1984). Reactive intercalating molecules such as urea and formamide enter the interlayer spaces and expand the kaolinite layers, essentially making the clay into a single-layered mineral. Reactive molecules have been classified into groups according to the point of clay interaction. Group A consists of compounds that form strong hydrogen bonds to the silicon tetrahedral sheets, for example, hydrazine, urea, formamide and acetamide (Lagaly 1984). Group B is made up of molecules with strong dipole interactions that can interact with the silicate layers, and includes molecules such as dimethyl sulphoxide that can provide considerable 3-dimensional order (Thompson 1985; Rapauch et al. 1987). Group C consists of the alkali salts of short-chain fatty acids, in particular, acetic and propionic acids (Weiss et al. 1966). In this study, one example from group A and one from group C have been selected for an intercalation study with a highly ordered halloysite.

Raman spectroscopy of the kaolinite clay minerals has been limited in extent (Wiewióra et al. 1979; Johnston 1985; Michaelian 1986). Recently Raman microscopy has been used to study halloysites (Frost et al. 1996; Frost and Shurvell 1997). Fourier transform Raman spectroscopy has been shown to be very useful for the study of the kaolinite clay mineral structure (Frost et al. 1993; Frost 1995, 1997). Although the technique of Raman microscopy has been in existence for some time (Dhamelincourt et al. 1979; Dubessy et al. 1982), the application of the Raman spectroscopic technique to the study of clay mineral structure has been limited. Clays are extremely weak Raman scatterers, and the Raman spectra of clays are very weak in intensity. Often the noise combined with background fluorescence means that spectra quality is lacking. The advent of low-energy near-infrared lasers that reduce the fluorescent background, and the use of charge-coupled detectors (CCD) that improve signal to noise, have meant that the Raman microprobe can be used for the analysis of minerals.

The advantage of using Raman spectroscopy is that bands in the 100 to 400 cm^{-1} region are easily measured. Such bands are not easily obtained using Fourier transform infrared (FTIR) techniques. Conventional dispersive Raman spectroscopy inherently has the clay spectrum superimposed on the intense Rayleigh line, particularly if an excitation at 532 nm is used. The use of Raman microscopy employing CCDs is greatly advantageous because of signal-to-noise improvement. Both FT Raman spectrometers and con-

ventional dispersive instruments are shot-noise limited. With a CCD detector, this is no longer true, and typically the noise from a detector is at least 100 times less than that from a semiconductor detector. One of the disadvantages of the use of the CCD detector is that it is susceptible to cosmic radiation which can at times interfere with the collection of spectral data. However, because the spectra of the kaolinite clay minerals, as for other minerals, are obtained in short periods of time, the problem is easily overcome by repeating the data collection. The disadvantage of using Raman spectroscopy operating at the diode laser frequency of 788 nm is the loss of efficiency. The Raman scattering decreases as the 4th power of the wavelength of the excitation radiation, so the efficiency of the Raman scattering at 788 nm compared to 532 nm, for example, is ~5 times less. For the 633-nm (HeNe) laser, this factor is 2 times less. Nevertheless, the disadvantage of this loss of efficiency is greatly outweighed by the advantages of the CCD detector. Furthermore, the advantages of using lasers operating in the 633- or 780-nm range rest with the reduction of the laser-induced fluorescence, which is a problem when using the green or blue regions of the spectrum. In particular, because of increased sensitivity and reduced noise levels, Raman microscopy may be used for the study of clay minerals. To date, however, there have been no reports on the Raman spectroscopy of intercalated halloysites. This paper reports the investigation of the structure of an halloysite and its intercalates using Raman spectroscopy.

EXPERIMENTAL

Preparation of Intercalates

The halloysite used in this study was from Szeg, Hungary. Samples were analyzed for phase purity using X-ray diffraction (XRD) techniques before Raman microprobe spectroscopic analysis. Some quartz and traces of a potassium feldspar and smectite were observed. Quartz was removed by sedimentation techniques, and the halloysite was dried in a desiccator to remove adsorbed water and used without further purification. The initial sample was designated Sample B. The urea intercalate was prepared by simply mixing 300 mg of halloysite with 30 mL of a 10 *M* urea solution. The urea solution was maintained at concentrations less than saturation, thus ensuring that no urea was mixed in with the halloysite-urea intercalate. This sample was designated Sample B1. The air-dried halloysite was intercalated with potassium acetate according to Weiss et al. (1963). Three hundred milligrams of halloysite were treated with 30 mL of 7.2 *M* potassium acetate solution. This sample was designated Sample B2. The samples were shaken for 80 h in a constant temperature bath at 65 °C for urea and at ambient temperature for potassium acetate. The excess solution on the clay was removed by centrifugation. The intercalated halloysite was allowed to dry in air for 5 d before Raman spectroscopic analysis. The halloysite urea complex was dried in a desiccator above anhydrous calcium chloride.

Raman Microprobe Spectroscopy

Microgram amounts of the samples were placed on a polished metal surface on the stage of an Olympus BHSM light microscope equipped with 10×, 20× and 50× objectives. No other sample preparation was needed. It was found that the best method of placing the halloysite on this metal surface was to take a very small amount on the end of the spatula and then tap the crystals onto the metal surface. Bundles of crystals of the halloysite intercalates were easily observed under the microscope. The microscope is part of a Renishaw 1000 Raman microscope system, which also includes a monochromator, a filter system and a CCD. Raman spectra were excited by a Spectra-Physics model 127 He/Ne laser (633 nm), or a diode laser (780 nm), and recorded at a resolution of 2 cm^{-1}. Spectra were acquired either in sections, approximately 1000 cm^{-1} for 633-nm excitation, or 800 cm^{-1} for 780-nm excitation. The microscope was designed around a light microscope, enabling switching from visible light to the laser excitation radiation. Repeated acquisitions using the highest magnification were accumulated to improve the signal-to-noise in the spectra. Spectra were calibrated using the 520.5-cm^{-1} line of a silicon wafer. This calibration is ideal for the study of the lattice region of kaolinite polymorphs. For the hydroxyl stretching region, calibration was done by using the peak position of the inner hydroxyl of kaolinite itself and positioning the band at 3620 cm^{-1}.

Spectral manipulations such as baseline adjustment, smoothing and normalization were performed using the Spectracalc software package GRAMS (Galactic Industries Corporation, New Hampshire). Band component analysis was carried out using the peakfit software by Jandel Scientific. Lorentz-Gauss cross-product functions were used throughout and peak fitting carried out until correlation coefficients with r^2 greater than 0.995 were obtained.

X-ray Diffraction

The XRD analyses were carried out on a Philips wide-angle PW 1050/25 vertical goniometer equipped with a graphite diffracted beam monochromator. Low-background silica plates were used. The *d*-spacing and intensity measurements were improved by application of a self-developed computer-aided divergence slit system enabling constant sample irradiation area (20 mm long) at any angle of incidence. The goniometer radius was enlarged from 173 to 204 mm. The radiation used was Cu$K\alpha$ from a long fine-focus Cu tube, operating at 40 kV and 40 mA. The samples were

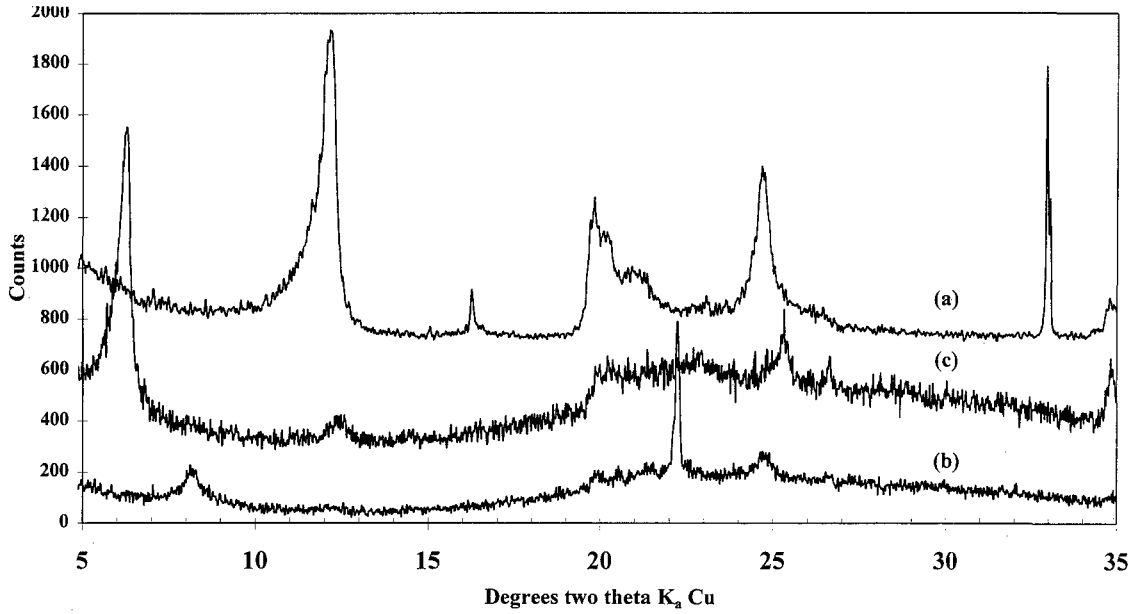

Figure 1. XRD patterns of (a) halloysite, (b) halloysite–urea intercalate, (c) halloysite–potassium acetate intercalate.

measured in stepscan mode from as low as 0.5 °2θ with steps of 0.02 °2θ and a counting time of 2 s. Measured data were corrected for the Lorentz polarization factor (for oriented specimens) and for their irradiated volume.

RESULTS AND DISCUSSION

X-ray Diffraction

The XRD of the Szeg halloysite showed a *d*(001) spacing of 7.207 Å (Figure 1). It was found that the halloysite was 90% intercalated for the halloysite-potassium acetate intercalate and 95% for the halloysite-urea intercalate. The crystal domain size from the 001 peak was 156 Å, implying that 22 layers are stacked in the halloysite crystal. The average crystal domain size was determined to be 231 Å. When the halloysite was intercalated with urea, the *d*-spacing became 10.762 Å. Only the 001 spacing was altered, and the spacings for the other 010 and 100 dimensions remained unchanged. The XRD analysis clearly showed a well-expanded halloysite of uniformity. The Scherer calculation provided information on the thickness along the *c* axis of 364 Å. This means that on average, there were 34 layers in 1 coherently diffracting crystal. When the halloysite was intercalated with potassium acetate, the *d*-spacing became 13.87 Å. Again, the other spacings remained unchanged, showing that the expansion of the halloysite layers occurred in 1 direction only, that is, along the *c* axis. However, the XRD analysis could not identify the presence of potassium acetate in the halloysite–potassium acetate intercalate. Thus, the crystal structure of the intercalating molecule had changed so much that a search for the spacings of potassium acetate could not be found. This observation could be explained in terms of the potassium acetate no longer being crystalline.

Raman Microscopy

Raman spectra are normally superimposed on a background, which is a combination of the fluorescence and the instrument function. In the case of the HeNe laser and the measurement of the hydroxyl stretching region, the background is predominantly due to fluorescence and consists of a sloping linear baseline that can be corrected easily. In the case of both the HeNe and the diode laser, the background for lattice region is predominantly the instrumental and depends on the detector response and the behavior of the filters. Although the background is a complex function, it can be measured easily by determining the white-light background, using the incandescent light from the microscope. The measured spectra are then ratioed to this instrumental background to give the spectra shown in this paper. Such a method ensures that the correct instrumental function is taken into account and that the true spectrum is measured. Different instrumental profiles are obtained for the operation of the 2 lasers. The filters of the 633-nm laser (HeNe) cut in at 100 cm^{-1}, making the recording of the spectra in the 50 to 150 cm^{-1} range difficult. The use of the 780-nm laser is better for determination of the bands between 100 and 150 cm^{-1}, as the filters start removing the Rayleigh line at lower frequencies.

Data collection times in the case of conventional dispersive Raman spectroscopy and, to a lesser extent, Fourier transform Raman spectroscopy, can be very

https://doi.org/10.1346/CCMN.1997.0450407 Published online by Cambridge University Press

long. Often several thousand spectra must be added to obtain a spectrum of sufficient quality. In the case of Raman microprobe spectroscopy, data collection times are very short and spectra are easily obtained within 1 to 10 min. Typically a collection time of 60 s is used with the ×50 magnification and 10 spectra coadded. Power at the sample is in the 1-mW power range. The spot size of the laser is ~1 μm^2. This use of such low power in Raman microprobe spectroscopy is a major advantage, particularly in comparison to FT Raman spectroscopy, where typically the power used for clays is 100 mW. Low power minimizes the heating effects and consequent damage to the clay mineral.

One of the disadvantages of Raman microprobe analysis is the fluorescence of the clay minerals, which is particularly pronounced when using the HeNe laser at 633 nm and with lasers of similar wavelengths. Each of the laser lines used to excite the Raman spectra of the kaolinite polymorphs caused fluorescence which subsided with time. Often 24-h exposure of the sample in the laser beam reduced this fluorescence to a minimum. Even so, no difficulty of measuring the lattice region with the 633-nm excitation was experienced. If the crystals were smaller than the spatial resolution of the microscope (1 μm), then spectra were obtained from an area that covered several crystals and an average spectrum was obtained.

Halloysite Hydroxyl Region

As with the other kaolin group minerals, halloysite contains 2 types of hydroxyl groups: 1) the outer hydroxyl groups, designated OuOH and 2) the inner hydroxyl groups, designated InOH. The OuOH groups are situated in the outer, unshared plane, whereas the InOH groups are located in the inner shared plane of the octahedral sheet. In an ordered kaolinite, such as the Georgia kaolinite (KGa-1), the 4 distinct infrared bands have been assigned as follows: the 3 higher-frequency vibrations (ν_1, ν_2, ν_3) are due to the 3 outer or so-called "surface" hydroxyls (OuOH), and the band at 3620 cm^{-1} is due to the InOH (Johnston et al. 1990). In halloysite, unlike the other kaolin group minerals, these OuOH groups may not necessarily be hydrogen-bonded to the next layer. As a consequence, the halloysite crystals assume morphologies different from that of kaolinite. The 3620-cm^{-1} IR band for kaolinite has been assigned to the InOH based on selective deuteration studies (Ledoux 1964; Wada 1967; White 1970; Rouxhet et al. 1977). In this paper's discussion of intercalated halloysites, this convention is adopted, and the additional bands are simply defined as ν_x, as they appear in the spectra. These InOH are bound to the Al atoms and extend towards the intralayer cavity of the kaolinite (Hess and Saunders 1992). For kaolinites, the InOH plane essentially lies parallel to the 001 plane and calculations predict the OH group to be at an angle of +3.1 degrees to this plane (Hess and Saunders 1992). This hydroxyl points towards the vacant octahedral site in the kaolinite dioctahedral structure (Collins and Catlow 1991). There is considerable debate as to the exact position of this InOH group in kaolinites, and it is possible that the position of the group depends on whether the Al-O-H bond is linear or bent. In halloysites, to the best of our knowledge, there have been only limited theoretical studies to define the halloysite structure (Singh 1996). Nevertheless, the width of the InOH Raman band suggests that a similar type of analysis is relevant to the study of halloysite structure.

The commonly accepted view is that the ν_1 and ν_2 bands are the coupled antisymmetric and symmetric vibrations (Brindley 1986; Michaelian 1986). The assignment of the ν_3 band is open to question, but the suggestion has been made that the band is due to symmetry reduction from an inner surface hydroxyl (Farmer and Russell 1964). The ν_2 and ν_3 bands of halloysite tend to form an almost continuous profile in the 3640 to 3680 cm^{-1} region. A description of bands in this region in terms of continuous states may be more applicable. Thus this is evidence that the OuOH groups do not take up a well-defined position, as occurs with kaolinites. Furthermore, it has been shown using both Raman (Pajcini and Dhamelincourt 1994; Johnston et al. 1985) and FT Raman spectroscopy (Frost 1995) that a 5th band at 3684 cm^{-1} exists which is also photoacoustic infrared active (Friesen 1986). This band has been attributed to an uncoupled inner surface hydroxyl that is not infrared active. This band is designated ν_4 in this work. Such bands are not observed in the IR spectra of kaolinite, although a band at 3684 cm^{-1} was clearly identified in the low-temperature infrared spectra of Prost (Prost 1989). This band is not observed in halloysites. The spectra are further complicated by the apparent existence of more than 1 OuOH ν_1 band for some kaolinite polymorphs (Frost 1997). It has been suggested that this phenomenon results from more than 1 kaolinite structural type in the sample: for example 1 kaolinite is ordered and the 2nd disordered.

Figure 2 shows a) the Raman spectra of the halloysite, b) the urea–halloysite intercalate, c) the potassium acetate halloysite intercalate, d) the kaolinite–urea intercalate and e) the kaolinite–potassium acetate intercalate. The band component analysis for the untreated halloysite is illustrated in Figure 3 and the results of this analysis are given in Table 1. The inner surface hydroxyl stretching region consisted of 3 OuOH groups defined as ν_1, ν_2 and ν_3, centered at 3696, 3675 and 3655 cm^{-1}. The ν_1 band contributed 41% of the total intensity of the normalized hydroxyl band intensity. It was noticeable that the prominent Raman band at 3684 cm^{-1} for ordered kaolinites was absent from the spectra of this halloysite. The Raman spectrum of Szeg halloysite was typical of an halloysite with a

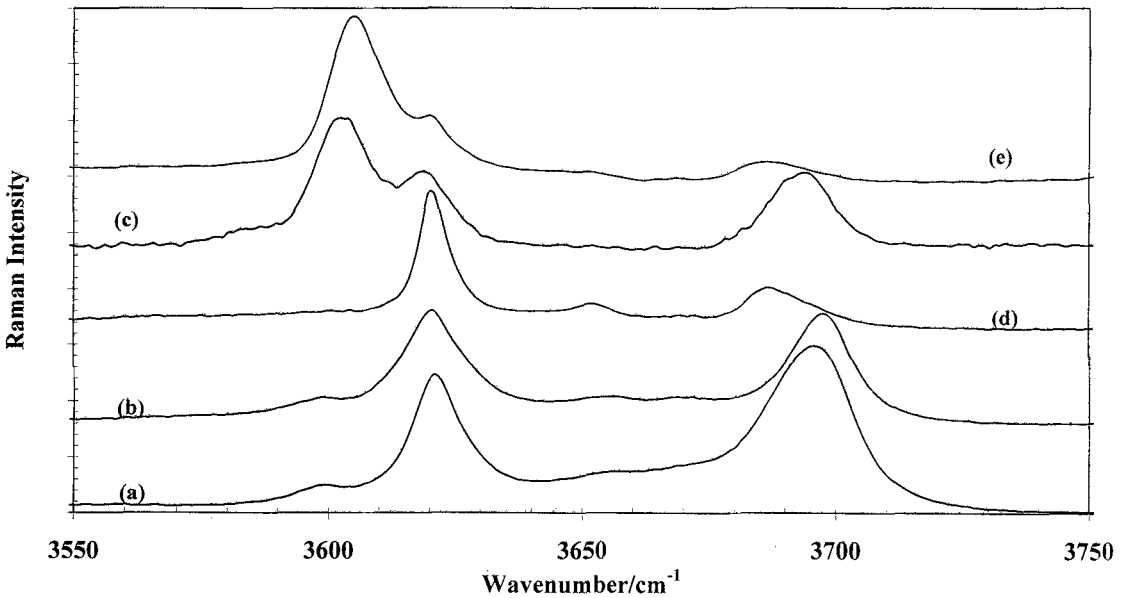

Figure 2. Raman spectra of the hydroxyl stretching region of (a) halloysite (sample B), (b) halloysite intercalated with urea (sample B1), (c) halloysite intercalated with potassium acetate (sample B2), (d) kaolinite–urea intercalate and (e) kaolinite–potassium acetate intercalate.

broad intense band at 3696 cm^{-1} and full width at half maxima (FWHM) of 9.5 cm^{-1}. Halloysites have been shown to have at least 2 bands in the 3620–3630 cm^{-1} region (Frost and Shurvell 1997). The band assigned to the InOH group at 3621 cm^{-1} was sharp with an FWHM of 5.7 cm^{-1}. A 2nd band defined as ν_6 was observed in this region at 3635 cm^{-1}, which made up approximately 7% of the total intensity. Two additional bands were observed at 3600 and 3555 cm^{-1}. These bands were due to the hydroxyl stretching of water hydroxyls. The band at 3600 cm^{-1} (ν_7) was attributed to intercalated water and the band at 3555 cm^{-1} (ν_8),

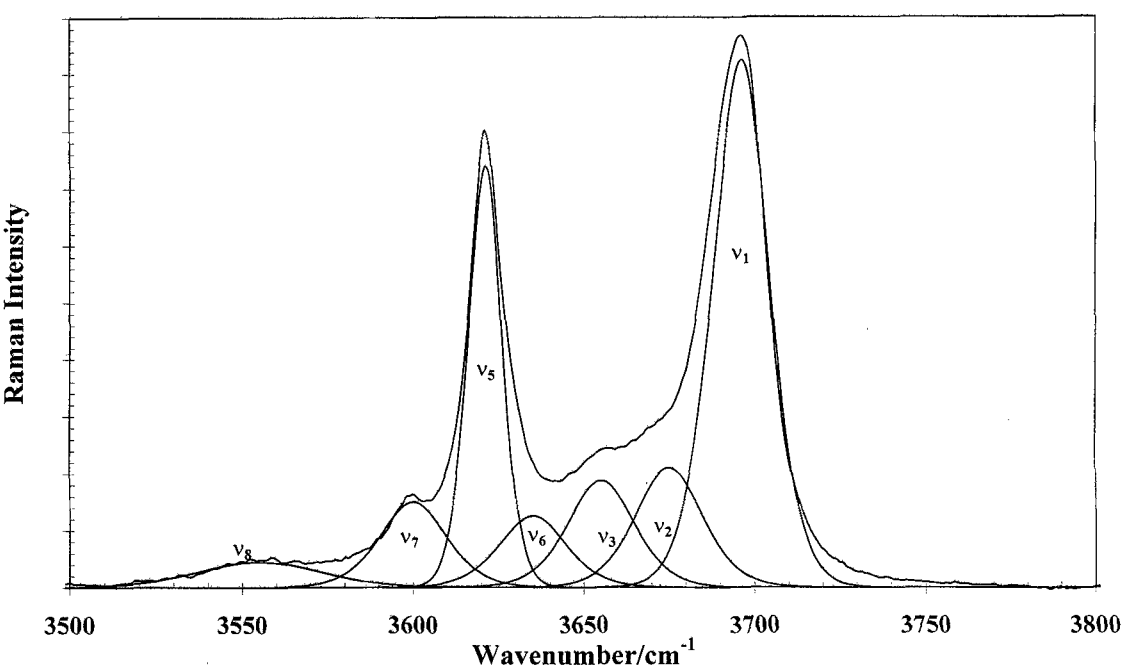

Figure 3. Band component analysis of the hydroxyl stretching region of halloysite.

https://doi.org/10.1346/CCMN.1997.0450407 Published online by Cambridge University Press

Table 1. Band positions, FWHM and band areas of the hydroxyl stretching region of halloysite sample B, halloysite intercalated with urea sample B1 and halloysite intercalated with potassium acetate sample B2.

Sample	Band center cm^{-1}	Band FWHM cm^{-1}	% area
B			
ν_8	3555	21	4.2
ν_7	3600	11.5	7.9
ν_5	3621	5.7	19.5
ν_6	3635	11.5	6.6
ν_3	3655	11.5	9.9
ν_2	3675	11.0	11
ν_4	—	—	—
ν_1	3696	9.5	40.7
B1			
Intercalated urea	3387	14.1	11.9
Intercalated urea	3410	14.3	11.9
ν_8	3497	23.5	10.2
ν_7	3598	8.6	5.0
ν_5	3620	7.6	22.6
ν_6			
ν_3	3653	11.0	6.8
ν_2	3672	11.5	6.0
ν_4			
ν_1	3696.5	8.5	25.5
B2			
ν_7	3585	7.5	6.85
ν_6	3602.5	5.7	39.0
ν_5	3619	6.7	26
ν_3	—	—	—
ν_2	—	—	—
ν_4	3686	7.8	7.9
ν_1	3695	6.2	20.5

to adsorbed water. Both of these bands were broad, with full band widths of 11.5 cm^{-1} for ν_7 and 21 cm^{-1} for ν_8. They contributed 12% of the total normalized band areas. If these 2 bands are removed from the area analysis, then the area of the InOH ν_5 band at 3621 cm^{-1} comprises 22% of the total normalized band area and the ν_1 band of the OuOH groups comprises 46.3% of the total band area. The other 3 vibrational modes, ν_2, ν_3 and ν_6, then comprise 31% of the total band area.

Intercalation of Halloysite with Urea

The Raman spectrum of the halloysite–urea intercalate is labeled (b) in Figure 2 and the amine stretching region for both urea and the halloysite–urea intercalate is shown in Figure 4. Band component analysis of the hydroxyl stretching region for the halloysite–urea intercalate is shown in Figure 5. Spectral data are given in Table 1. A comparison of the spectra of the halloysite and the halloysite–urea intercalate revealed Raman bands at 3387, 3410 and 3497 cm^{-1} for the halloysite intercalate. The observed bands in this region are due to the formation of hydrogen bonds between the N-H of the urea and another group. Therefore, these bands were attributed to the formation of a urea-Si_2O_5 complex. The 3600-cm^{-1} band remained unchanged. The band profile in the IR reflectance spectra consisted of a very broad profile with the halloysite hydroxyl bands superimposed. The advantage of Raman spectroscopy lies with the resolution of the NH and OH bands. The ν_1 band at 3696 cm^{-1} had a width of 8.5 cm^{-1}. This band was somewhat sharper for the intercalate compared with the untreated halloy-

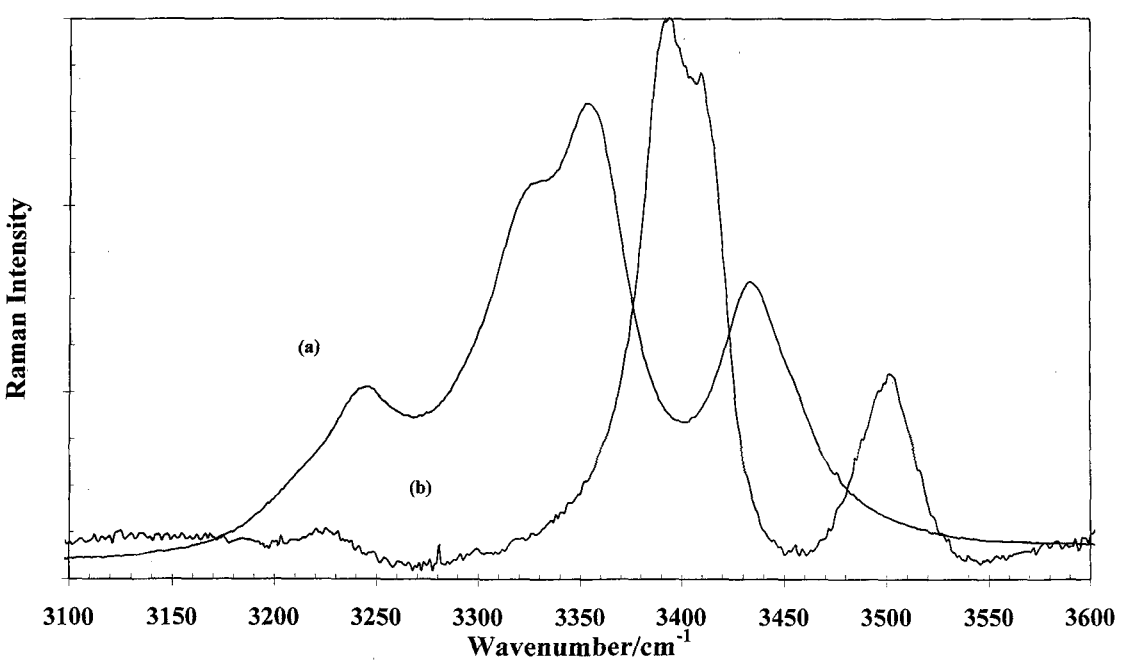

Figure 4. Raman spectrum of halloysite and the urea–halloysite intercalate in the N-H stretching region.

https://doi.org/10.1346/CCMN.1997.0450407 Published online by Cambridge University Press

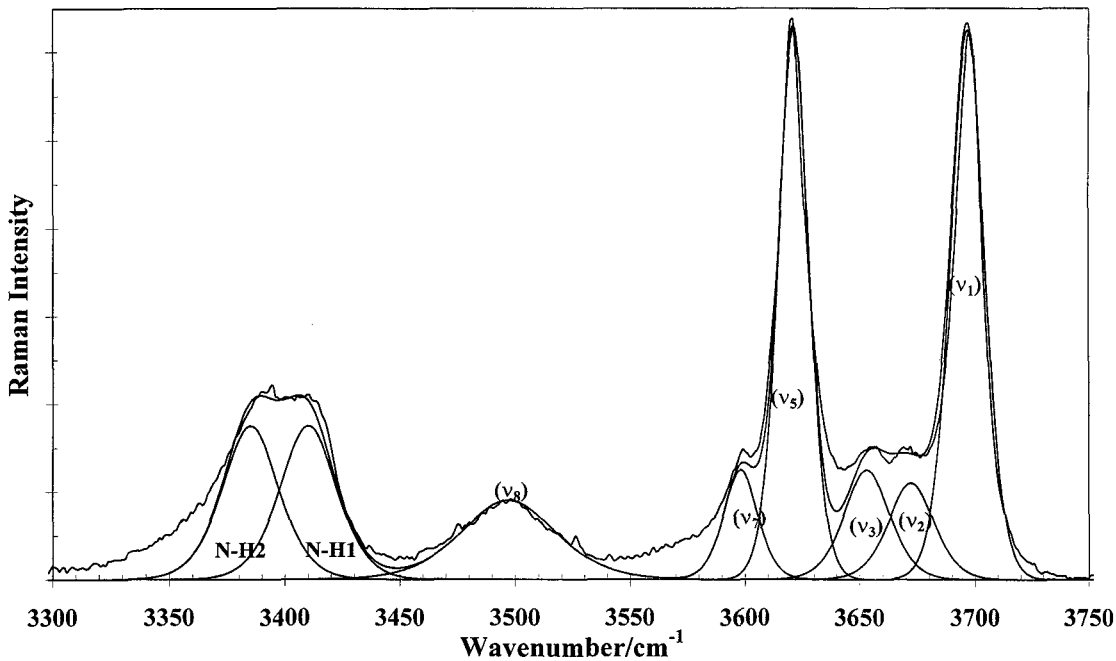

Figure 5. Band component analysis of the hydroxyl stretching region of halloysite–urea intercalate.

site. The urea bands and ν_7 and ν_8 made up 40% of the total band area in this region. Bands ν_7 and ν_8 were Raman active only. No peaks at 3497 or 3410 cm^{-1} occurred in the IR reflectance spectra. A vibration that has a Raman active mode and an inactive infrared mode has a center of symmetry. It is proposed that the 3497-cm^{-1} band resulted from a highly symmetric -N-H–O-Si- unit of the urea–silicon tetrahedral sheet.

Considering only the halloysite hydroxyl bands, then the intensity of the InOH ν_5 band increased from 22.1 to 37% of the total normalized band area. The intensity of the OuOH ν_1 band decreased from 46.3 to 42.5% of the total normalized band area. The areas of the ν_5 and ν_1 bands were of a similar magnitude and the spectrum of the urea–halloysite intercalate closely resembled that of a urea-intercalated kaolinite, (d) on Figure 2. This can be expected, as the effect of the intercalating molecule is to delaminate halloysite and transform the halloysite into a single-layer kaolinite polymorph, even though the intercalating molecule itself may form hydrogen bonds between the layers. On intercalation of the halloysite with urea, remarkable intensity changes in the hydroxyl stretching bands occured. The relative intensity of the OuOH groups was reduced. This reduction was attributed to the loss of hydrogen bonding of the inner surface hydroxyl groups. The intercalated urea disrupted the interlayer hydrogen bonding between the kaolinite layers by the formation of hydrogen bonds between the Si-O of the silicon tetrahedral sheets and the N-H of the urea. This was indicated by the appearance of new urea bands of relatively high intensity at 3387 and 3410 cm^{-1}. Pure urea has bands at 3244, 3327, 3353 and 3433 cm^{-1}. The bands at 3387 and 3410 were attributed to the symmetric and antisymmetric stretching modes of the N-H of the urea molecule.

The spectra of the low-frequency region of the halloysite, the urea–halloysite intercalate and the potassium acetate–halloysite intercalate are shown in Figure 6. The results of the analyses are reported in Table 2. The spectrum of the halloysite–urea intercalate resembled that of the untreated halloysite. New bands were observed at 583 and 1009 cm^{-1} and were attributed to urea vibrational modes. Pure urea has very weak Raman bands at 133 and 172 cm^{-1} and stronger bands at 544 and 1007 cm^{-1}. The band at 544 cm^{-1} shifted to 583 cm^{-1} in the intercalate. This band was due to the N-H libration and this large increase in the band center was attributed to the formation of strong hydrogen bonds between the N-H of the urea and the Si-O of the halloysite tetrahedra, which resulted in a more restricted libration. A good comparison could be made between the Raman spectra of urea and the urea–halloysite intercalate in the 1100 to 1800 cm^{-1} region. The band at 1679 cm^{-1} attributed to the symmetric stretching vibration of the C=O group was not observed in the intercalate. A shift in the CN symmetric stretching frequency from 1464 to 1468 cm^{-1} was observed. A marked increase in intensity of the 1540-cm^{-1} band was noted and was attributed to an increase in symmetry of the H-N-H bend as the N-H groups are hydrogen-bonded to the silicon tetrahedral sheet.

https://doi.org/10.1346/CCMN.1997.0450407 Published online by Cambridge University Press

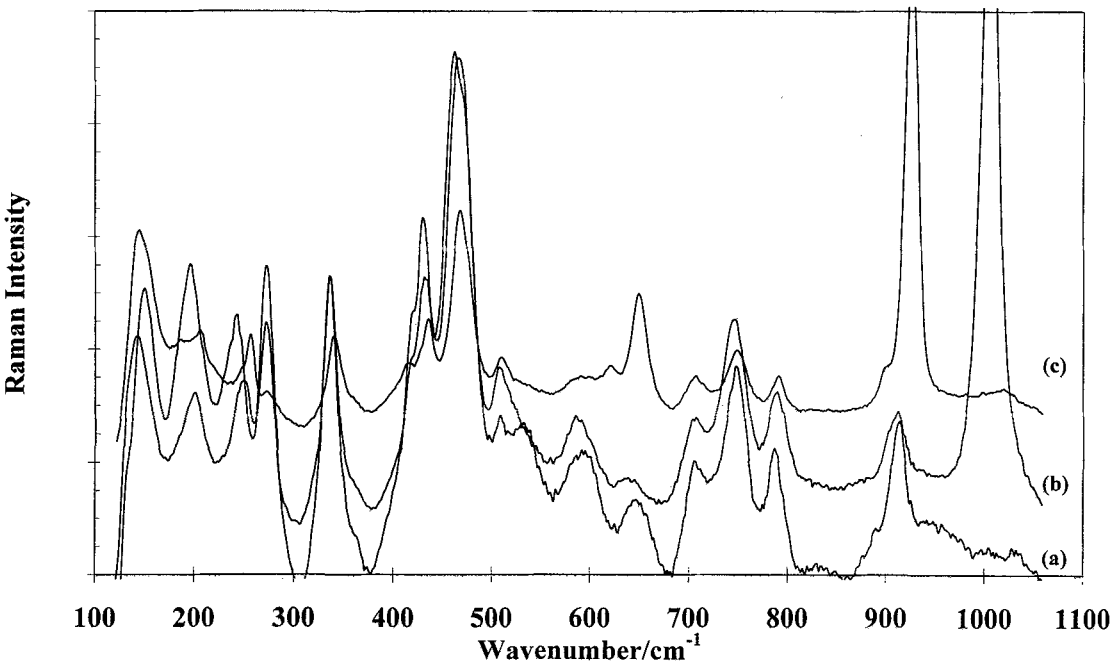

Figure 6. Raman spectra of the low-frequency region of (a) halloysite, (b) halloysite–urea intercalate, (c) halloysite–potassium acetate intercalate.

A decrease in the relative intensities of the bands attributed to urea at 1176 and 1640 cm^{-1} was observed.

Changes in the Al-OH librational modes of halloysite also occurred (Figure 7). The Al-OH libration in most kaolinites is observed as 2 bands at 916 and 936 cm^{-1}. For the urea intercalate, these 2 bands shifted to 905 and 914 cm^{-1}. The shift in these bands was attributed to the loss of hydrogen bonding of the Al-OH groups. Other changes were observed in the $\nu_4(f_2)$ mode of the SiO_4 tetrahedron, where a marked increase in the intensity of the band occured, which was again attributed to the formation of hydrogen bonds between the Si-O tetrahedra and the N-H of the urea. Changes were also observed in the $A_{1g}(\nu_1)$ mode of AlO_6 octahedron at 200 cm^{-1} and the $B_2(\nu_3)$ mode of O-H-O triangle at 243 cm^{-1}. The 1st band showed complexity and is diminished in intensity. The 2nd band showed considerable increase in intensity and also shifted from 243 to 252 cm^{-1}. The 2 vibrational modes of the SiO_4 tetrahedra at 432 and 462 cm^{-1} shifted to 438 and 464 cm^{-1} and were considerably broadened. These changes were again attributed to the formation of the hydrogen bonds between urea and silicon tetrahedra.

Table 2. Raman spectral results of the lattice modes of halloysite, halloysite intercalated with urea and halloysite intercalated with potassium acetate.

Suggested assignment	Halloysite band position cm^{-1}	Halloysite–urea intercalate band position cm^{-1}	Halloysite–potassium acetate intercalate band position cm^{-1}
$\nu_2(e)$ of AlO_6 octahedron	143	143	151
$A_{1g}(\nu_1)$ of AlO_6 octahedron	200	192	195
$B_2(\nu_3)$ of O-H-O triangle	243	249	252
$A_1(\nu_1)$ of O-H-O triangle	272.5	272	—
$\nu_2(e)$ of SiO_4 tetrahedron	336	335	340
$\nu_2(e)$ of SiO_4 tetrahedron	—	—	353
$\nu_2(e)$ of SiO_4 tetrahedron	—	—	397
$\nu_4(f_2)$ of SiO_4 tetrahedron	432	433	438
$\nu_4(f_2)$ of SiO_4 tetrahedron	462	464	464
$\nu_4(f_2)$ of SiO_4 tetrahedron	512	509	509
Intercalated urea band	—	583	—
Intercalated acetate	—	—	621
Intercalated acetate	—	—	645
Si-O-Al translation	647	—	648
Si-O-Al translation	710	709	705
Si-O-Al translation	747	745	748
OH translation	787	789	788
OH libration	913	912	925
Intercalated urea mode	—	1009	—

Intercalation of the Halloysite with Potassium Acetate

The Raman spectrum of the hydroxyl stretching region of the potassium acetate intercalated halloysite is labeled (c) in Figure 2 and the band component analysis of the Raman spectrum of the hydroxyl stretching region is shown in Figure 8. Spectral details are reported in Table 1. The remarkable feature of the spectrum was the very large increase in the ν_6 band centered at 3602.5 cm^{-1}. This band made up 39% of the

https://doi.org/10.1346/CCMN.1997.0450407 Published online by Cambridge University Press

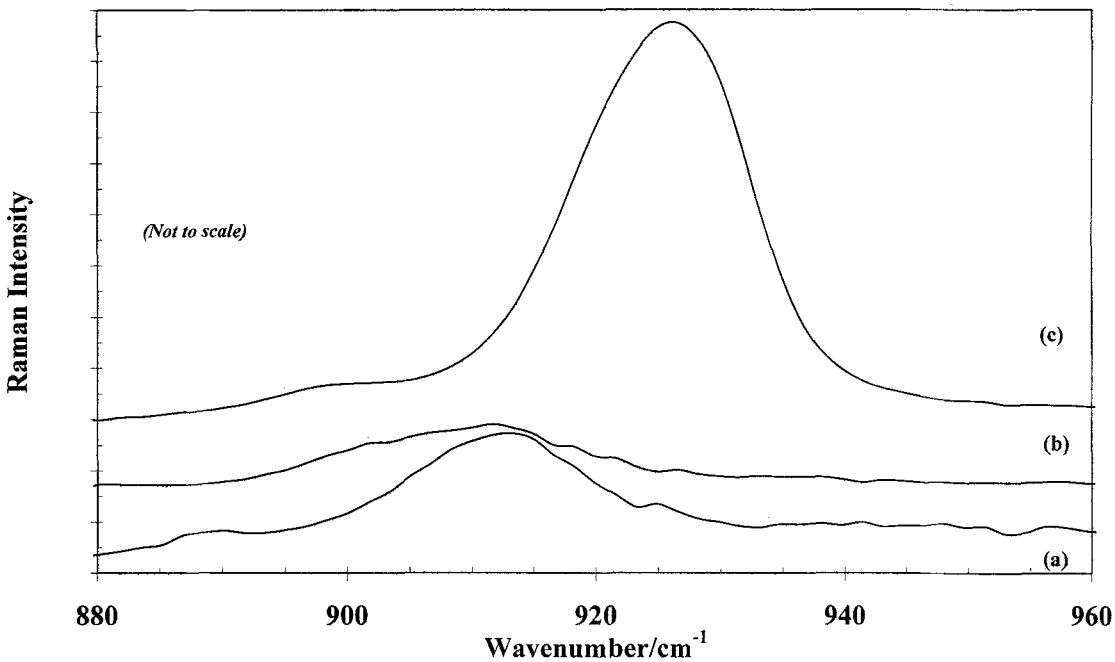

Figure 7. Raman spectra of the Al-OH libration for (a) halloysite, (b) halloysite–urea intercalate, (c) halloysite–potassium acetate intercalate.

total normalized band area and was sharp with an FWHM of 5.7 cm^{-1}. This band was also observed in the IR reflectance spectrum at 3600 cm^{-1} and was broad. Furthermore, a 2nd band apparent at 3585 cm^{-1}, defined as ν_7, made up 7% of the total normalized band area with an FWHM of 7.5 cm^{-1}. Such a band was not observed in the spectra of either halloysite or the halloysite–urea intercalate. This band was Raman active only. Such a band results from a vibration that possesses a center of symmetry.

The Raman spectrum for the halloysite–potassium acetate intercalate, (c) on Figure 2, was remarkable on

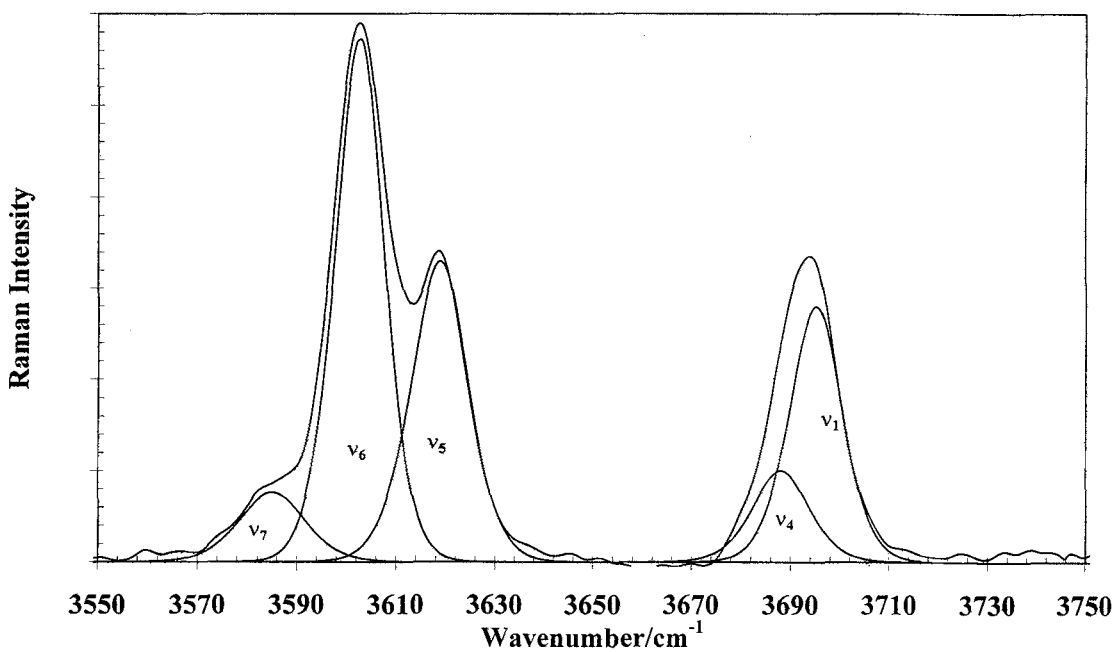

Figure 8. Band component analysis of the hydroxyl stretching region of halloysite–potassium acetate intercalate.

https://doi.org/10.1346/CCMN.1997.0450407 Published online by Cambridge University Press

3 counts: 1) intensity of the ν_2 and ν_3 bands was zero, 2) the spectrum strongly resembled that of an intercalated kaolinite, (e) on Figure 2, and 3) the bands were remarkably sharp. The ν_4 band that was not detected in the spectrum of the untreated halloysite made up 8% of the total normalized band intensity. The ν_1 and ν_4 bands also narrowed and had band widths of 6.2 and 7.8 cm^{-1}. The intercalation process caused definition of these particular vibrational modes. In comparison with the untreated halloysite, the intensity of the ν_1 band decreased from 46.3 to 20.5%. This decrease was accounted for by the formation of the bands at 3602.5 and 3585 cm^{-1}. These changes, in all probability, resulted from the formation of hydrogen-bonded complexes between the OuOH groups and the potassium acetate molecule.

The lattice spectrum of the potassium acetate intercalated halloysite is labeled (c) on Figure 6 and the spectral results are reported in Table 2. A comparison between the spectra of the halloysite and the halloysite intercalates showed remarkable changes in the lattice vibrational modes. The most significant change was the remarkable increase in the intensity of the Al-OH librational mode for the potassium acetate intercalate shown in Figures 6 and 7. The spectra for this region showed complexity. In the untreated halloysite, the Al-OH librational spectral region showed complexity with 3 bands at 906 and 913 cm^{-1} with an additional band at 888 cm^{-1}. In the urea intercalate, these bands were observed at 898, 905 and 915 cm^{-1} and were attributable to the Al-OH librational modes. The fact that there are 3 vibrations for this mode was a consequence of the nonequivalence of the Al-OH groups. It was proposed that this nonequivalence arises from the folding of the halloysite layers (Singh 1996). In the potassium acetate intercalate, bands were found at 925, 915 and 896 cm^{-1}. For the potassium acetate intercalate, the 925-cm^{-1} band area was 95% of the total band area with the 915-cm^{-1} band area 4% and the 896-cm^{-1} band area 1% of the total normalized band area. The 936-cm^{-1} band has been attributed in IR spectroscopy to the librational mode of the OuOH groups (Farmer 1974). The band showed a 10-fold increase in intensity and was depolarized with a depolarization ratio of 0.55. Such observations were attributed to a highly symmetric vibration. It was proposed that, during the intercalation process, the OuOH groups had their hydroxyl groups realigned from a wide variety of angles in the original halloysite to an angle approaching 90° to the 001 face of the potassium acetate intercalate. The Raman spectrum in the hydroxyl stretching region of the halloysite–potassium acetate intercalate strongly resembled that of a kaolinite–potassium acetate intercalate, (c) and (e) on Figure 2. Such an observation supports the view that, on a molecular scale, there is little difference between the structure of an intercalated halloysite and an intercalated kaolinite. Thus it can be questioned if the intercalating molecule provides a mechanism, at least on the molecular scale, for the conversion of an halloysite to a kaolinite.

The next significant change was in the ν_2(e) mode of the AlO_6 octahedron at ~140 cm^{-1}. The band profile in this region showed complexity, and the changes in this spectral region for the 3 samples studied are shown in Figure 9. The untreated halloysite showed a prominent band at 143 cm^{-1} with a shoulder at 130 cm^{-1}. The spectra of the halloysite–urea intercalate showed bands at 143 and 152 cm^{-1} with a weak additional band at 129 cm^{-1}. Spectra of the halloysite–potassium acetate intercalate showed 2 bands at 151 and 156 cm^{-1} with an additional weak band at 132 cm^{-1}. The Raman bands in the 129 to 130 cm^{-1} region have been attributed to the O-Si-O symmetric bending mode (Frost 1995). The bands at 151 and 156 cm^{-1} showed an increase in intensity and were polarized with a depolarization ratio of 0.62. The band at ~200 cm^{-1} for the pure halloysite was attributed to the A_{1g} (ν_1) mode of the AlO_6 octahedra and showed complexity with at least 2 bands at 197 and 192 cm^{-1}. This band for the urea intercalate had almost no intensity. The band for the potassium acetate intercalate was a single vibration with a band center at 195 cm^{-1}. Such an observation was attributed to the equivalence of the OuOH groups, that is, the differences in the OuOH groups have been removed due to formation of the intercalate. The OuOH groups that correspond to the ν_1, ν_2 and ν_3 vibrational modes were no longer distinguishable and all OuOH groups were in the same direction. The bands at 243 and 272 cm^{-1} were attributed to the $B_2(\nu_3)$ mode of O-H-O triangle and the $A_1(\nu_1)$ mode of O-H-O triangle. These bands were identical for the untreated halloysite and the urea intercalate. These bands were considerably diminished in intensity in the spectrum of the potassium acetate intercalate.

The band at 336 cm^{-1} that has been attributed to the ν_2(e) mode of the SiO_4 tetrahedron was diminished in intensity and showed complexity in the spectrum of the intercalate. The band was again identical in the spectra of both halloysite and the halloysite–urea intercalate. The band shifted to 340 cm^{-1} for the halloysite–potassium acetate intercalate. The formation of the intercalate removed the hydrogen bonds formed between the Si-O tetrahedra and the OuOH groups of the next kaolin layer. Intercalation caused the kaolin layers to separate due to the insertion of the intercalating molecule. The layers, however, were still bonded to the next layers via the intercalant. The 400 to 520 cm^{-1} region characterizes the Si-O symmetric stretching region and, typically for kaolinite polymorphs, is characterized by 2 bands at 429 and 464 cm^{-1} with an additional band at 512 cm^{-1}. Overlap of the symmetric stretching band from quartz impurity

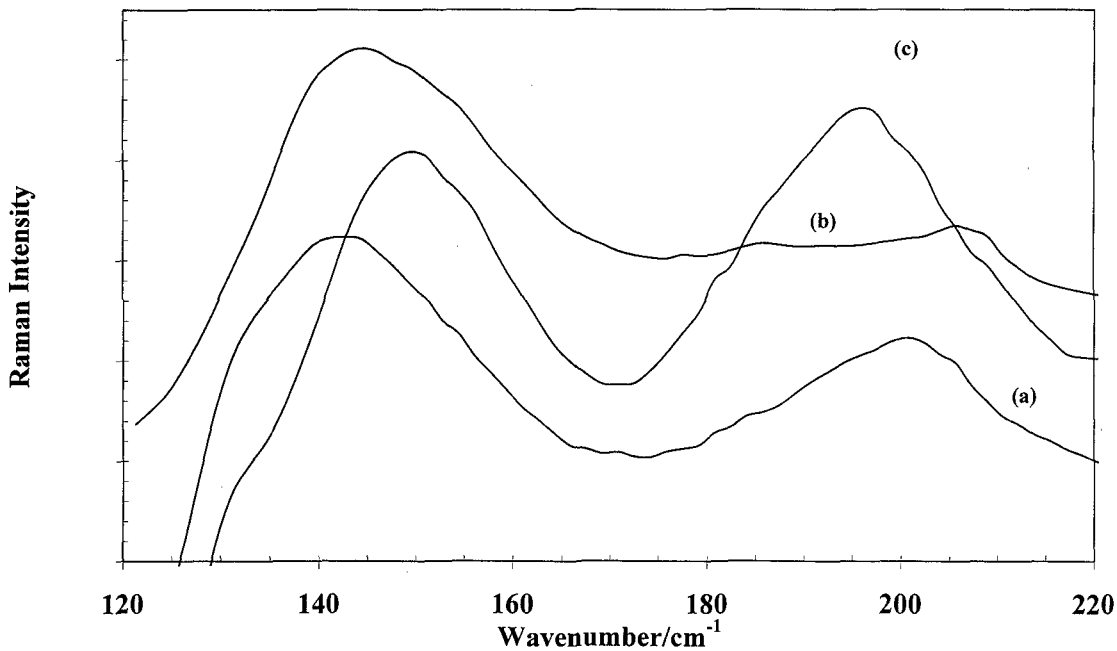

Figure 9. Raman spectra of the 120 to 220 cm^{-1} region of (a) halloysite, (b) halloysite–urea intercalate and (c) halloysite–potassium acetate intercalate.

can interfere, particularly with the 464-cm^{-1} band of the kaolinites. The band at 429 cm^{-1} showed complexity with a shoulder in all 3 spectra at 415 cm^{-1}. The 464-cm^{-1} band also showed complexity with 2 bands at 464 and 472 cm^{-1}. This band was broadened in the spectra for halloysite–urea intercalate. Some of this complexity was not observed in the spectra of the halloysite–potassium acetate intercalate with the band at 472 cm^{-1} reduced in intensity. Multiple bands occurred from a loss of symmetry of the Si_2O_5 units. Changes were observed in this region on intercalation of the kaolinite with potassium acetate. Both the $\nu_4(f_2)$ modes at 464 and 512 cm^{-1} of the Si_2O_5 unit showed an increase in intensity on potassium acetate intercalation.

Remarkable changes in the acetate bands at 1420 and 1350 cm^{-1} are illustrated in Figure 10. The 1420 cm^{-1} band attributed to the $\nu_3(A_1)$ symmetric stretching vibration of the O-C-O unit shifted from 1420 to 1412 cm^{-1}. The band at 1352 cm^{-1} was attributed to the $\nu_6(e)$ deformation mode of the CH_3 group of the acetate (Kaklhana et al. 1983). The peak was a single sharp symmetric peak in the pure potassium acetate and became 2 peaks at 1355 and 1345 cm^{-1}. Further changes were observed in the $\nu_5(A_1)$ symmetric bend of the O-C-O acetate unit. Two bands were observed at 656 and 619 cm^{-1} in the Raman spectrum of pure potassium acetate, but in the spectrum of the potassium acetate intercalate there was only a single symmetric band at 648 cm^{-1}. The loss of symmetry of the CH_3 bending vibration would indicate the reason for 2 peaks. It is proposed that the CH_3 group of the acetate may be interacting with the silicon tetrahedral layer through the formation of weak hydrogen bonds between the C-H and the Si-O. Alternatively, the CH_3 groups are fitting into the spaces of the next adjacent kaolin layer with a consequential restriction in rotation. One methyl group is keyed into the ditrigonal hole in the tetrahedral sheet with the other Si-C bond parallel to the sheet. Evidence of such a proposal was found in the study of the kaolinite–dimethyl sulphoxide (DMSO) intercalates where the DMSO molecules are accommodated by significant horizontal displacement of individual kaolinite layers to achieve almost perfect overlap of the octahedral vacancy by the adjacent ditrigonal hole (Thompson 1985). Thus it would appear that the acetate is not only intercalating with the inner surface hydroxyls of 1 halloysite layer but also the silicon tetrahedral sheet of the next halloysite layer.

CONCLUSIONS

A sample of an ordered halloysite was intercalated with potassium acetate and urea. The potassium acetate intercalate showed a new very intense Raman band at 3602.5 cm^{-1} with a half width of 5.7 cm^{-1} and 2nd band at 3585 cm^{-1}. The normal halloysite modes of ν_1 to ν_3 showed remarkable decreases in intensity. Associated with these new bands were the consequential changes in the bands at 913 and 143 cm^{-1}, which have been attributed to the Al-OH librational and O-Al-O symmetric bending modes. These bands

https://doi.org/10.1346/CCMN.1997.0450407 Published online by Cambridge University Press

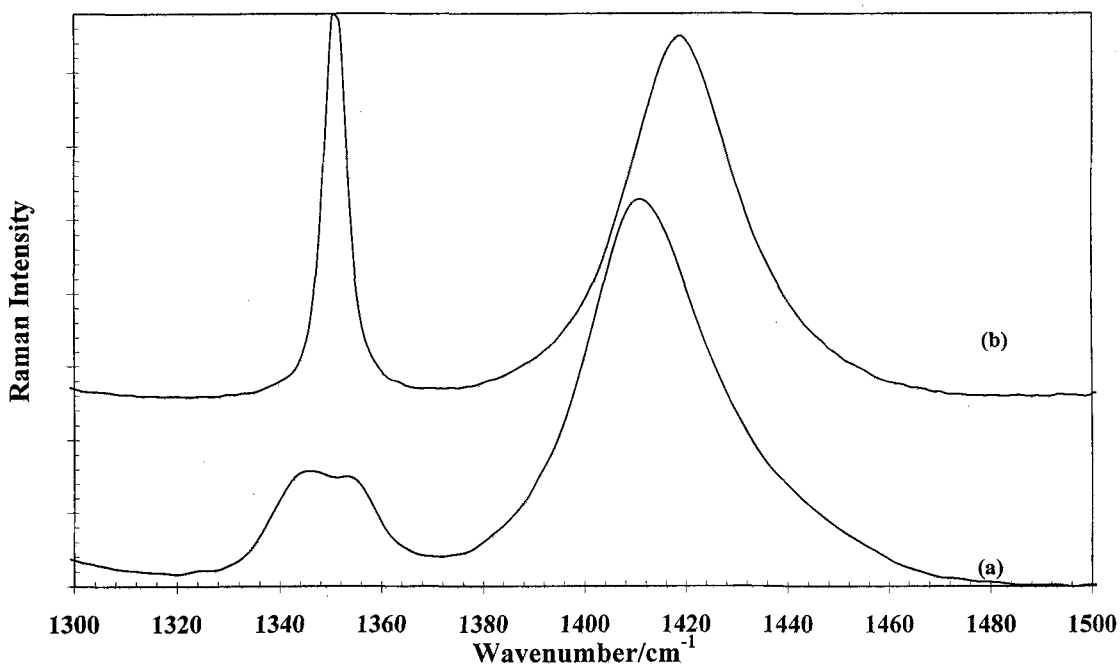

Figure 10. Raman spectrum of potassium acetate and halloysite–potassium acetate intercalate in the 1300 to 1500 cm^{-1} region.

showed an increase in intensity by an order of magnitude and the bands showed significantly high depolarization values. It is proposed that these changes are attributable to the OuOH groups being at an angle approaching 90° with the 001 face. Changes in the other lattice vibrations associated with O-H-O and Al-O-Si vibrations were also noteworthy. Further changes in the O=C=O and CH_3 deformation modes were observed. It was hypothesized that not only is the C=O group involved with the hydrogen bonding of the inner surface hydroxyls, but also the C-H groups are interacting with the silicon layer of the adjacent halloysite layer.

Intercalation of the halloysite with urea resulted in the formation of new urea Raman bands at 3387, 3410 and 3497 cm^{-1}. No new halloysite hydroxyl stretching bands were found. In contrast to the acetate intercalate, changes were observed in the spectroscopy of the Si_2O_5 units of the halloysite. In particular, changes were observed in the Al-OH librational modes and in the $\nu_4(f_2)$ and $\nu_2(e)$ of the SiO_4 tetrahedra. These changes were attributed to the hydrogen bonding of the NH_2 groups to the oxygen of the silicon tetrahedral sheets. Further substantial changes were observed in the urea vibrational modes at 544, 1007, 1464 and 1540 cm^{-1} bands. These changes were also accounted for in terms of the interaction of the urea NH_2 groups with the silicon tetrahedral layer.

Raman microscopy studies have shown 2 types of intercalation, as exemplified by: 1) the intercalation of halloysite with urea, with the molecule being hydrogen-bonded to 1 site of the halloysite lattice and 2) potassium acetate, the molecule being hydrogen-bonded not only to 1 site on the lattice, but also to a site of the next adjacent lattice. The intercalation of the halloysite with potassium acetate produced an intercalate with a Raman spectrum that strongly resembled that of an intercalated kaolinite. Thus, the intercalation process converted the halloysite structure to that of a kaolinite structure. Raman microscopy using a CCD and in combination with a 633-nm laser was shown to be very useful for the measurement of Raman spectra of halloysite and halloysite intercalates. Excellent-quality Raman spectra of the hydroxyl stretching bands and of the lattice modes of the intercalates were obtained. It was found that spectra of the halloysite intercalates were obtained with minimal collection times and with excellent signal-to-noise ratios. In this work, Raman spectroscopy has been shown to be a very useful technique for adding new insights into the structure of intercalated halloysites.

ACKNOWLEDGMENTS

S. Van der Gaast of the Netherlands Institute for Sea Research is thanked for many helpful discussions. A. Raftery of the Queensland University of Technology X-ray facility is thanked for carrying out the X-ray diffraction analyses. Dr. B. Singh of the Centre for Microscopy and Microanalysis of the University of Queensland is thanked for many helpful suggestions to the manuscript. Financial support from the Hungarian Scientific Research Fund under grant OTKA-T014179 is also acknowledged. The financial support of the Queensland University of Technology Centre for Instrumental

and Developmental Chemistry is also gratefully acknowledged.

REFERENCES

Brindley GW, Kao C, Harrison JL, Lipsiscas M, Raythatha R. 1986. Relation between the structural disorder and other characteristics of kaolinites and dickites. Clays Clay Miner 34:233–249.

Churchman GJ, Whitton JS, Claridge GGC, Theng BKG. 1984. Intercalation method using formamide for differentiating halloysite from kaolinite. Clays Clay Miner 32:241–248.

Collins DR, Catlow CRA. 1991. Energy minimised hydrogen atom positions of kaolinite. Acta Crystallogr Sect B47: 678–682.

Dhalemincourt P, Beny JM, Dubessy J, Poty B. 1979. Analysis of fluid inclusions with the MOLE Raman microprobe. Bull Mineral 102:600–610.

Dubessy J, Audeoud D, Wilkins R, Kostolyani C. 1982. The use of the Raman microprobe MOLE in the determination of the electrolytes dissolved in the aqueous phase of fluid inclusions. Chem Geol 37:137–150.

Farmer VC, Russell JD. 1964. The infrared spectra of layered silicates. Spectrochim Acta 20:1149–1173.

Farmer VC. 1974. The layer silicates. In: Farmer VC, editor. Infrared spectra of minerals. London: Mineral Soc. p 331–363.

Friesen WI, Michaelian KH. 1986. Fourier deconvolution of photoacoustic FTIR spectra. Infrared Physics 26:235–239.

Frost RL. 1995. Fourier transform Raman spectroscopy of kaolinite, dickite and halloysite. Clays Clay Miner 43:191–195.

Frost RL. 1997. The structure of the kaolinite clay minerals—An FT Raman study. Clay Miner 32:73–85.

Frost RL, Fredericks PM, Bartlett JR. 1993. Fourier transform Raman spectroscopy of kandite clays. Spectrochim Acta 20:1149–152.

Frost RL, Fredericks PM, Shurvell HF. 1996. Raman microscopy of some Kaolinite clay minerals. Can J Appl Spectrosc 41(1):10–14.

Frost RL, Shurvell HF. 1997. Raman microprobe spectroscopy of halloysite. Clays Clay Miner 45:68–72.

Hess AC, Saunders VR. 1992. Periodic *ab initio* Hartree-Fock calculations of the low-symmetry mineral kaolinite. J Phys Chem 96:4367–4374.

Janik LJ, Keeling JL. 1993. FT-IR partial least-squares analysis of tubular halloysite in kaolin samples from the Mount Hope kaolin deposit. Clay Miner 28:365–378.

Johnston CT, Agnew SF, Bish DL. 1990. Polarized single-crystal Fourier transform infrared microscopy of Ouray dickite and Keokuk kaolinite. Clays Clay Miner 38:573–583.

Johnston CT, Sposito G, Birge RR. 1985. Raman spectroscopic study of kaolinite in aqueous suspension. Clays Clay Miner 33:483–489.

Kaklhana M, Kotaka M, Okamoto M. 1983. Vibrational analysis of the acetate ion molecules and estimation of equilibrium constants for their hydrogen isotope exchange reactions. J Phys Chem 87:2526–2535.

Lagaly G. 1984. Clay organic reactions. Phil Trans R Soc Lond. A311:315–332.

Ledoux RL, White JL. 1964. Infrared study of selective deuteration of kaolinite and halloy site at room temperature. Science 145:47–49.

Ledoux RL, White JL. 1967. Infrared study of intercalation complexes of kaolinite. Silicates Ind 32:269–273.

Michaelian KH. 1986. The Raman spectrum of kaolinite #9 at 21 °C. Can J Chem 64:285–289.

Olejnik S, Aylmore LAG, Posner AM, Quirk JP. 1968. Infrared spectra of kaolin mineral–dimethyl sulfoxide complexes. J Phys Chem 72:241–249.

Pajcini V, Dhamelincourt P. 1994. Raman study of the OH-stretching vibrations in kaolinite at low temperature. Appl Spectrosc 48:638–641.

Prost R, Damene AS, Huard E, Driard J, Leydecker JP. 1989. Infrared study of structural OH in kaolinite, dickite nacrite and poorly crystalline kaolinite at 5 to 600K. Clays Clay Miner 37:464–468.

Raupach M, Barron PF, Thompson JG. 1987. Nuclear magnetic resonance, infrared, and X-ray powder diffraction study of dimethylsulfoxide and dimethylselenoxide intercalates with kaolinite. Clays Clay Miner 35:208–219.

Rouxhet PG, Samudacheata N, Jacobs H, Anton O. 1977. Attribution of the OH stretching bands of kaolinite. Clay Miner 12:171–178.

Singh B. 1996. Why does halloysite roll?—A new model. Clays Clay Miner 44:191–196.

Theng BKG, Churchman GJ, Whitton JS, Claridge GG. 1984. Comparison of intercalation methods for differentiating halloysite from kaolinite. Clays Clay Miner 32:249–258.

Thompson JG, Cuff C. 1985. Crystal structure of kaolinite: Dimethyl sulfoxide intercalate. Clays Clay Miner 33:490–500.

Wada K. 1967. A study of hydroxyl groups in kaolin minerals utilising selective deuteration and infrared spectroscopy. Clay Miner 7:51–61.

Weiss A, Thielepape W, Orth H. 1966. Intercalation into kaolinite minerals. In: Heller L, Weiss A, editors. Proc Int Clay Conf. Jerusalem: Israel Univ Pr. p 277–293.

Weiss A, Thielepape W, Ritter W, Schafer H, Goring G. 1963. Zur Kenntnis von hydrazin-kaolinit. Anorg Allg Chem 320: 183–204.

White JL, Laycock A, Cruz M. 1970. Infrared studies of proton delocalisation in kaolinite. Bull Groupe Franc Argiles 22:157–165.

Wiewióra A, Wieckowski T, Sokolowska A. 1979. The Raman spectra of kaolinite subgroup minerals and of pyrophyllite. Arch Mineral 135:5–14.

(Received 19 May 1996; accepted 15 September 1996; Ms. 2768)